*Kovove Mater. 62 2024 303–312*
*DOI: 10.31577/km.2024.5.303*



# Research on the microstructure and electrical conductivity in hypereutectic Al-Si compacts and $B_4C$ added composites fabricated by conventional, microwave, and spark plasma sintering

Melika Ozer*

*Metallurgical and Materials Engineering, Faculty of Technology, Gazi University, 06560, Ankara, Turkey*

Received 29 June 2024, received in revised form 27 October 2024, accepted 30 October 2024

**Abstract**

In the present study, hypereutectic Al-Si alloy compacts and Al-Si/$B_4C$ composites were produced by conventional, microwave, and spark plasma sintering techniques. The effects of sintering techniques and $B_4C$ particle addition on microstructural properties, density, hardness, and electrical conductivity were investigated. The microstructures were examined with an optical microscope. Densities were measured using the Archimedes technique. Electrical resistance measurements were made using the four-point probe measurement technique. Elemental Al grains, master alloy grains, and primary Si particles were determined in the microstructures of all samples. The addition of 15 wt.% $B_4C$ caused the porosity rate to increase in the samples. Samples produced with the SPS technique gave ≈ 80 % higher hardness values than samples produced with CS and MWS. Compared to the samples produced with CS and MWS, the samples produced with SPS gave higher electrical conductivity values. Electrical conductivities were decreased as the weight percentage of $B_4C$ increased in all samples.

K e y w o r d s: sintering, electrical conductivity, composite, Al alloy, microstructures

## 1. Introduction

Composite materials, whose most important advantages are their light weight and high mechanical properties, are used in aerospace, military, automobiles, etc. Advanced engineering materials are widely used in industries [1–4]. The high specific strength of composite materials has increased the interest in composite materials [5–7]. Composites with high specific strength can be produced using aluminum alloys as matrix materials. Hypereutectic Al-Si alloys have recently been preferred as matrix materials due to their high wear resistance and strength [8–11].

Composite materials are produced using different powder metallurgy (P/M) techniques. P/M technique in general: The process consists of powder production, mixing the powders produced, and pressing and sintering the powders. Cold pressing and sintering (conventional sintering (CS)) are the most generally known P/M techniques [12, 13]. Sintering is a heat treatment process that causes particles to bond, resulting in high density, increased strength, and improved properties [14–16]. Recent research on composite material production has focused on sintering techniques that save energy and time. Microwave sintering (MWS), spark plasma sintering (SPS), laser sintering, and induction sintering are energy and time-saving sintering techniques [6, 17, 18]. SPS is a powder compression and sintering technique. Among the advantages of SPS are a high heating rate, low sintering temperature, short sintering time, and no need for pre-compression. MWS offers the opportunity to perform sintering in shorter times than CS with the advantage of a high heating rate. With suitable sintering techniques, matrix materials, and reinforcement elements, end-product composite materials that can meet specific needs at a high rate can be designed and produced with energy and time savings [9, 19].

While composite material production produces materials with high specific strength, the electrical conductivity of the matrix material is compromised. Electrical conductivity provides a lot of information

*Corresponding author: e-mail address: mcerah@gazi.edu.tr

Table 1. Chemical composition of Alumix® 231 (wt.%) and pressing-sintering conditions

| | | Al | Si | Cu | Mg | Lubr. Amidwax |
|---|---|---|---|---|---|---|
| Alumix® 231 | Nominal target: | Remainder | 14–16 | 2.4–2.8 | 0.5–0.8 | 1.5 |
| | Experimental: | Remainder | 15.10 | 2.75 | 0.60 | |
| | Compacting pressure: 620 MPa<br>Sintering temperature: 550–560 °C<br>Sintering time: approx. 60 min | | | | Sintering atmosphere: $N_2$<br>Dewaxing: 380–420 °C | |

about the chemical purity and mechanical properties of the material. Electrical conductivity helps predict other properties, such as thermal conductivity, that are more difficult to determine [19, 20]. Electrical conductivity is very sensitive to the microstructure of metallic materials. While alloying element atoms, crystal structure defects, and reinforcing ceramic particles increase the mechanical strength of metals, they negatively affect electrical conductivity [19–21].

Suppose composites with high mechanical properties can be produced without compromising electrical conductivity and/or with minimal compromise, materials with high specific strength and good electrical conductivity that will meet performance expectations can be obtained. This study investigated the effects of the production method and $B_4C$ particle addition on the microstructural properties, densities, hardness, and electrical conductivity properties of samples produced with different P/M techniques. Hypereutectic Al-Si alloy powders were chosen as matrix materials due to their good mechanical and thermo-physical properties, such as high specific strength, low thermal expansion coefficients, high thermal conductivity, and good wear and corrosion resistance [22–24]. Boron carbide particles in the $B_4C$ composition, an attractive reinforcement element with superior properties such as high hardness, wear resistance, and low density, were used as reinforcement elements [25, 26]. Hypereutectic Al/Si alloy compacts and Al-Si/$B_4C$ composites were produced using CS, MWS, and SPS techniques. These three sintering techniques with different production parameters were compared. The advantages of SPS and MWS, which are rapid sintering techniques, over each other are discussed. The advantages of SPS and MWS over CS were examined by considering the microstructure, density, hardness, and electrical conductivity properties. In addition, the effects of % $B_4C$ used in composite production on microstructure, density, hardness, and electrical conductivity are discussed.

## 2. Materials and methods

In this experimental study, hypereutectic Al-Si compacts and 5–15 wt.% $B_4C$ reinforced hypereutectic Al-Si matrix composites were produced by CS, MWS, and SPS techniques. A pre-alloyed mixture of hypereutectic Al-Si powders produced by ECKA Granulate Velden GmbH with the trademark Alumix® 231 was used as the matrix material. The average sizes ($D_{50}$) of Alumix® 231 powders and $B_4C$ particles are $\sim 75$ and $\sim 10$ μm, respectively. The chemical composition and recommended pressing-sintering conditions of Alumix® 231 are given in Table 1.

5 and 15 % $B_4C$ by weight were added to Alumix® 231 powders to produce particle-reinforced composite materials. The prepared powders were blended for 45 minutes in a triaxial mixer, Turbula T2F brand/model device. Powders prepared for CS and MWS processes were cold pressed by applying 620 MPa pressure with a 200-ton capacity, a unidirectional hydraulic press. The lubricant elimination process was applied to the pressed samples and those prepared for SPS to remove the lubricant contained in Alumix® 231. This process was completed by holding time for 20 min at 400 °C.

CS process was carried out using a tube furnace in an $N_2$ atmosphere at a heating rate of 5 °C min$^{-1}$ and at a temperature of 555 °C. The holding time at the sintering temperature was 60 min, and the samples were cooled in air. The MWS process was conducted in a Synotherm brand atmosphere-protected laboratory-type microwave oven with a heating rate of 10 °C min$^{-1}$. The samples were sintered at a sintering temperature of 555 °C and held for 15 min at this temperature. Studies conducted on Alumix® 231 stated that the sintered density increased with increasing sintering temperature up to 560 °C. It has been stated that sintering at temperatures above 560 °C causes loss of density. They attributed the decrease in sintered density to the increasing liquid phase volume, the liquid phase regions coalescing to form large pools, and these liquid pools forming pores during cooling [27–29]. Therefore, the sintering temperature of 555 °C was chosen for the CS and MWS processes.

For SPS, 25 g of powder was charged into the mold, and a preload of 1 MPa was applied. The powders were sintered at 450 °C for 5 min by applying 50 MPa pressure. The SPS process was carried out in a vacuum environment at a heating rate of 100 °C min$^{-1}$. Table 2 illustrates the specimen notations of the samples.

Table 2. The specimen notations of the samples

| Specimen notation | Materials | Sintering | Sintering temperature (℃) | Sintering time (min) |
|---|---|---|---|---|
| CS-555/60 | Alumix® 231 | Conventional | 555 | 60 |
| 5-CS-555/60 | Alumix® 231 +5 wt.%$B_4C$ | Conventional | 555 | 60 |
| 15-CS-555/60 | Alumix® 231 +15 wt.%$B_4C$ | Conventional | 555 | 60 |
| MWS-555/15 | Alumix® 231 | Microwave | 555 | 15 |
| 5-MWS-555/15 | Alumix® 231 + 5 wt.%$B_4C$ | Microwave | 555 | 15 |
| 15-MWS-555/15 | Alumix® 231 + 15 wt.%$B_4C$ | Microwave | 555 | 15 |
| SPS-450/5 | Alumix® 231 | Spark plasma | 450 | 5 |
| 5-SPS-450/5 | Alumix® 231 + 5 wt.%$B_4C$ | Spark plasma | 450 | 5 |
| 15-SPS-450/5 | Alumix® 231 + 15 wt.%$B_4C$ | Spark plasma | 450 | 5 |

The samples were subjected to standard metallographic grinding and polishing processes for microstructural analysis. Keller's reagent was used to etch the samples. The microstructures of the prepared samples were imaged and analyzed with an optical microscope. The phases formed after sintering processes were determined by X-ray diffraction (XRD) analysis (Bruker D8 Advance, Cu-K$\alpha$ ($\lambda = 1.54056$ Å)).

The densities of the sintered samples were measured by the Archimedes technique by the ASTM B962-08 standard. Densities are reported as relative density in proportion to the theoretical density value. Theoretical density was calculated according to the mixture rule using the material composition.

Macro hardness tests of the samples were performed using the Brinell hardness method (Emcotest Duravision). Hardness measurements were performed with a load of 31.5 kgf and a hardened steel indenter ball with a diameter of 2.5 mm. Ten measurements were carried out on each sample. The arithmetic averages of the measurement results were used.

Electrical resistance measurements were made at room temperature (300 K) to determine the electrical conductivity of the samples. Electrical resistance measurements were carried out using the four-point probe measurement technique. The four-point probe technique is a method used for low-level DC resistance measurement. It has high precision and contains less measurement error. In this technique, two probes are used to apply current to the material, and the other two are used to measure the voltage of the material. Measurements were made with a Keithley 2450 SourceMeter brand/model measuring device. Data were analyzed with Kickstart software version 2.10.1. Six current ($I$) and voltage ($V$) measurements were taken from each sample. The arithmetic averages of the data obtained were calculated. Then, respectively, the resistivity ($\rho$) and conductivity ($\sigma$) values were calculated for each sample using Eqs. (1) and (2):

$$\rho = \frac{V}{I} \cdot \frac{wh}{L}, \tag{1}$$

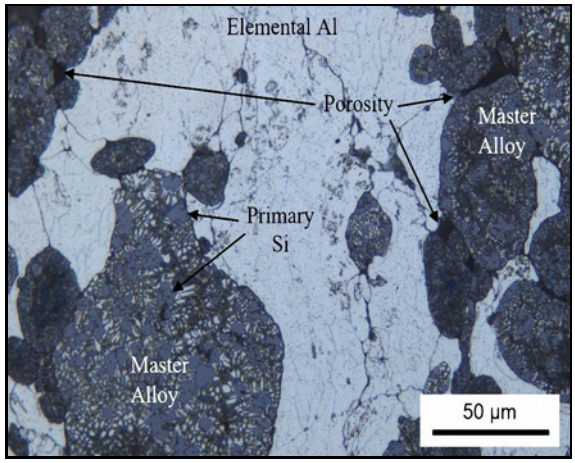


Fig. 1. Optical microscope micrograph of green Alumix® 231.

$$\sigma = \frac{1}{\rho}, \tag{2}$$

where $V$ is the voltage between the points where the probes contact the sample (V), $I$ is the current between the probes (A), $w$ is the sample width (m), $h$ is the height (m), $L$ is the distance between the points where the probes contact the sample (m).

## 3. Results and discussion

### *3.1. Material and microstructure characterization*

Commercial hypereutectic Al-Si powders and hypereutectic Al-Si/$B_4C$ mixture powders were cold pressed unidirectionally with 620 MPa pressure. Cold-pressed samples were sintered using CS and MWS techniques. In addition, commercial hypereutectic Al-Si and Al-Si/$B_4C$ mixture powders were sintered with the spark plasma technique, and compact samples were produced. Figure 1 shows the optical micro-

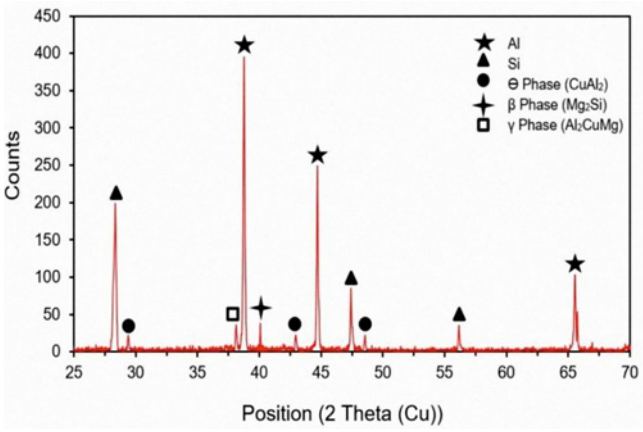


Fig. 2. The XRD patterns of SPS-450/5.

scope micrograph of green Alumix® 231. Alumix® 231 is a P/M powder consisting of elemental aluminum and original master alloy (Al-Si-Cu-Mg) powders. The light-colored areas in the micrograph in Fig. 1 are grains formed by elemental Al powders containing low amounts of Si, Cu, and Mg. The dark regions containing grayish coarse particles and fine bright particles are the original master alloy Al-Si-Cu-Mg composition. It is stated in the literature that grayish coarse particles are primary Si particles, and fine bright particles are Cu-rich secondary phases [10, 22, 30]. It has been stated in the literature that structures rich in Cu content have $\theta$ ($CuAl_2$) and $\gamma$ ($Al_2CuMg$) secondary phases and that the Mg element exists as the $\beta$ ($Mg_2Si$) secondary phase in the microstructure [7, 27, 31–33]. The phases formed in the sintered sample microstructure were determined by XRD analysis. The XRD graph of the SPS-450/5 sample is given in Fig. 2. By the literature, Al, Si phases and Cu-rich $\theta$ ($CuAl_2$), $\gamma$ ($Al_2CuMg$), and Mg-rich $\beta$ ($Mg_2Si$) secondary phases were determined by XRD analysis.

Optical micrographs of the samples are given in Fig. 3. It was determined from the micrographs that elemental Al grains, master alloy grains, and primary Si particles were formed in the microstructures of all samples, depending on the matrix material. Alumix® 231 is a pre-alloyed mixture powder consisting of a mixture of pure aluminum powders and Al-Si-Cu-Mg alloy powders. Si is an alloying element in the Al-Si-Cu-Mg master alloy powder. Si particles are formed as particles in the master alloy powder grains by sintering and are called primary Si.

CS and MWS samples gave porosity values close to each other. The porosity rates of CS-555/60, 5-CS-555/60, and 15-CS-555/60 samples were calculated as 11.95, 12.88, and 15.29 %, respectively. The porosity rates of MWS-555/15, 5-MWS-555/15, and 15-MWS-555/15 samples were calculated as 13.7, 13.81, and 15.06, respectively. The advantage of the MWS technique over the CS technique is that the heating rate is high, the holding time is short, and energy saving is achieved. However, approximately 12 % more porosity was determined in the microstructure of the compacts produced from pure Alumix® 231 with the MWS (MWS-555/15) technique compared to the sample produced with the CS (CS-555/60) technique.

In the MWS process, the holding time at the sintering temperature was very short, causing a lack of coalescence between the grains and causing more porosity in the MWS-555/15 sample. The addition of 5 wt.% $B_4C$ did not cause a significant change in the porosity ratio of the samples produced by CS and MWS techniques. Porosity rates of 11.95 and 13.7 % were determined in the microstructures of CS-555/60 and MWS-555/15 samples. In microwave sintering, heat is generated internally within the material rather than from external sources; hence, there is an inverse heating profile [34]. Unlike conventional heating, microwave heating converts electromagnetic energy to thermal energy rather than heat transfer. Since the material is heated by energy conversion, heating is very rapid, and volumetric heating occurs. However, for microwave sintering to occur, the material must have the ability to absorb electromagnetic waves. In materials that can absorb electromagnetic waves, electromagnetic energy is converted into thermal energy. Since metals are opaque, they reflect electromagnetic waves from the material surface. Pressed powder metal parts provide partial penetration because they have a porous structure. This partial penetration of electromagnetic waves allows pressed powder metal samples to be sintered using the microwave technique [35–37]. Therefore, it is thought that in the sintering of powder metal parts with the microwave technique, a porous microstructure like conventional sintering is formed since not all microwave energy is converted into heat energy.

The pores formed in the microstructure after sintering the mixture powders prepared with the addition of 5 wt.% $B_4C$ by CS or MWS techniques are the places where $B_4Cs$ are located. In other words, $B_4C$ particles added to Alumix® 231 as a strengthener are located within the pores in the microstructure. Therefore, adding 5 wt.% $B_4C$ did not cause a significant change in the porosity rate. The addition of 15 wt.% $B_4C$ caused an increase in the porosity rate in the samples. The porosity rates of the samples produced by sintering the mixture powders prepared by adding 15 wt.% $B_4C$ with CS and MWS increased by ≈27 % and ≈ 10 %, respectively. The high surface tension of $B_4Cs$ settled between elemental Al and/or master Al grains seen in Alumix® 231 micrographs caused porosity in these regions.

The samples with the lowest porosity rate are the samples produced with SPS (Fig. 3). Porosity rates in SPS-450/5, 5-SPS-450/5, and 15-SPS-450/5 samples

were calculated as 1.54, 2.79, and 4.81 %, respectively. SPS is a pressure sintering technique. This study carried out the SPS process at 450 ℃, 50 MPa pressure, and 5 min sintering time. In SPS, sparks formed at the contact points or gaps between the powders charged to the mold cause instantaneous regional high temperatures and, therefore, evaporation and melting on the surfaces of the powder grains. The pressure applied during sintering eliminates and/or minimizes microspaces between powder grains and/or $B_4C$ clusters [18, 38, 39].

When the micrographs of the SPS-450/5, 5-SPS-450/5, and 15-SPS-450/5 samples given in Fig. 3 are examined, it is seen that the amount of poros-

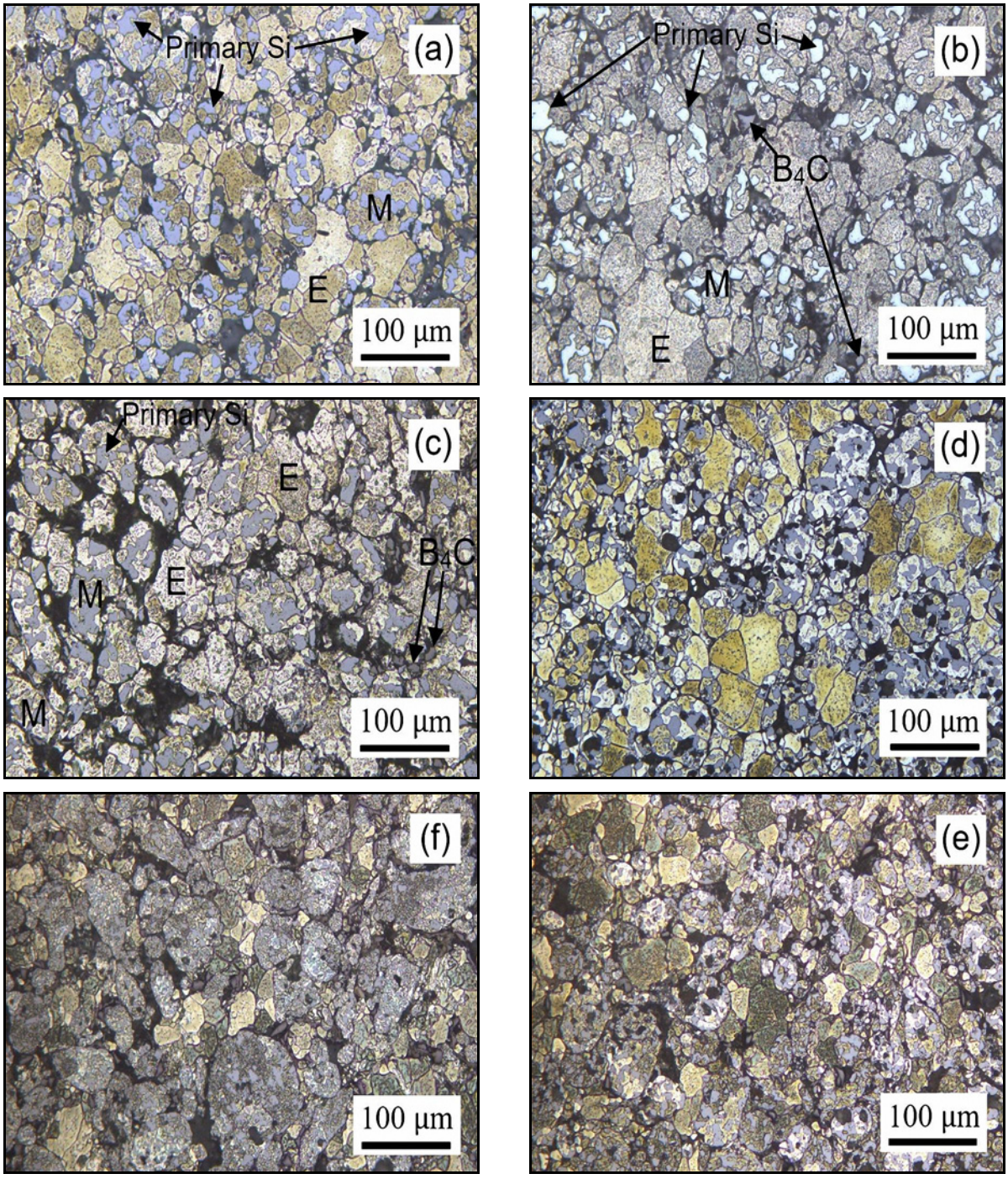


Fig. 3a–f. Optical micrographs of samples: (a) CS-555/60, (b) 5-CS-555/60, (c) 15-CS-555/60, (d) MWS-555/15, (e) 5-MWS-555/15, (f) 15-MWS-555/15.

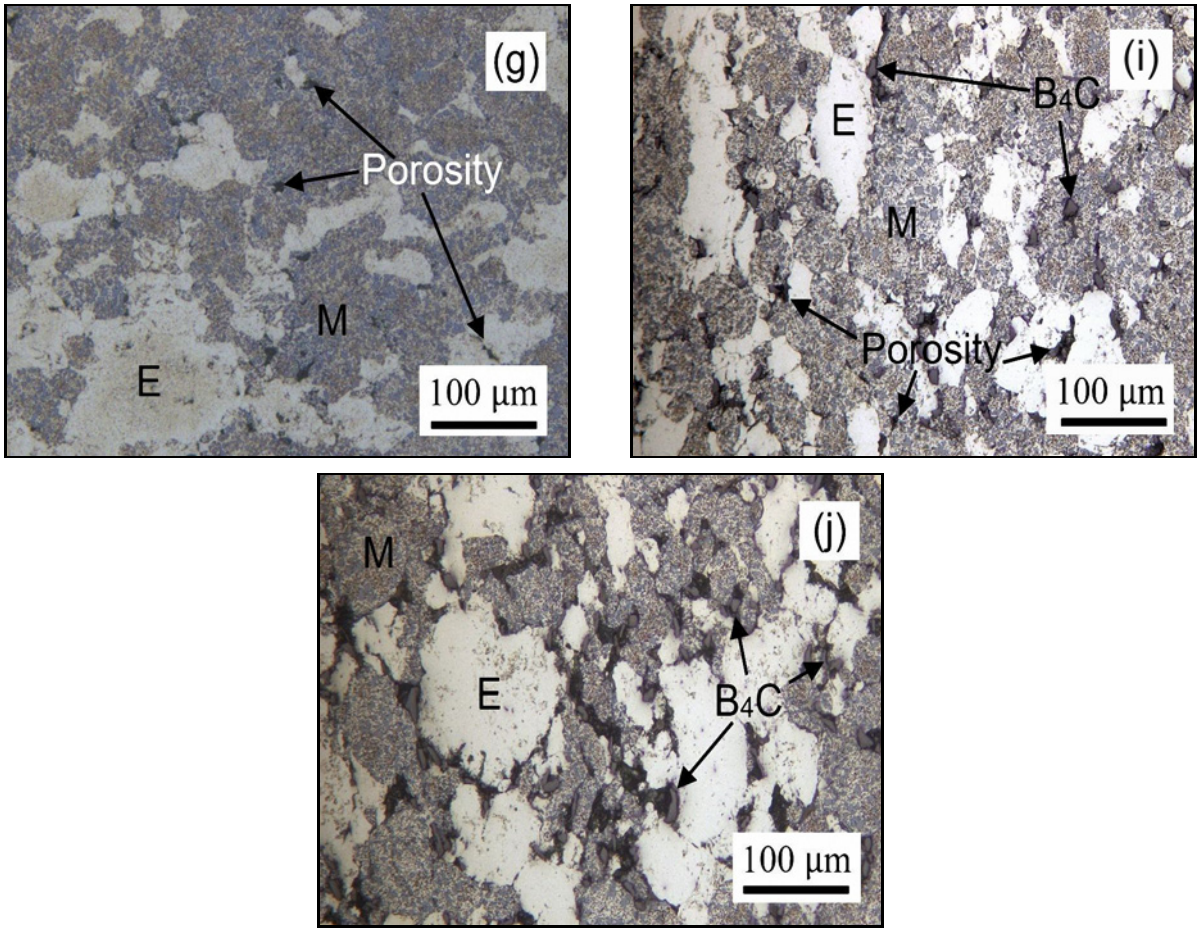


Fig. 3g–j. Optical micrographs of samples: (g) SPS-450/5, (i) 5-SPS-450/5, and (j) 5-SPS-450/5 (E: elemental Al grains; M: master alloy grains).

ity is quite low, and the existing pore size is smaller than other sintering techniques. The pores in the microstructure of the 15-SPS-450/5 sample have larger sizes than other SPS samples. The agglomeration of $B_4C$ particles can be said to be the reason for the formation of large pores. Moreover, the pre-compression pressure applied in the SPS technique and the sintering pressure applied during sintering (50 MPa in this study) directly affect the mechanical arrangement of the powder particles. The applied pressure rearranges the powder particles, deforms them, and increases their compressibility. The Alumix® 231 powders were produced by inert gas atomization, are nearly spherical, and have an average powder size of about 75 µm. $B_4C$ particles have irregular geometry (sharp corners), and the average particle size is $< 10$ µm. Therefore, Alumix® 231 powder particles with spherical geometry have good flow properties and compressibility. It can be said that $B_4C$ particles have worse flow properties and compressibility. Under the sintering pressure applied during SPS, Alumix® 231 powders, which have good flow and compressibility, can easily roll on each other, deform, and compress. Meanwhile, the hard $B_4C$ particles, which have poor flow and compressibility and cannot be deformed, agglomerate due to their strong cohesive (tensile) properties caused by their small size. The agglomerated $B_4C$ particles are pushed towards the matrix grain boundaries by the Alumix® 231 powders, which have high flow and compressibility properties. The increase in porosity with the addition of 15 wt.% $B_4C$ is attributed to the incompatibility between the matrix grains and $B_4C$ particles and the lack of a continuous and effective interface [18, 40]. The high matrix/particle size ratio (approximately 7.5) and the high surface energy of $B_4C$ ceramic particles caused more agglomeration of $B_4C$ particles in compacts containing 15 wt.% $B_4C$ in all sintering techniques.

### *3.2. Density and hardness*

Sample densities were measured using the Archimedes technique according to the ASTM B962-08 standard. Densities are reported as relative density. The hardness values of the samples were measured using the Brinell hardness type. The density and hardness of the samples are given in Fig. 4. In the samples produced with different sintering techniques, with

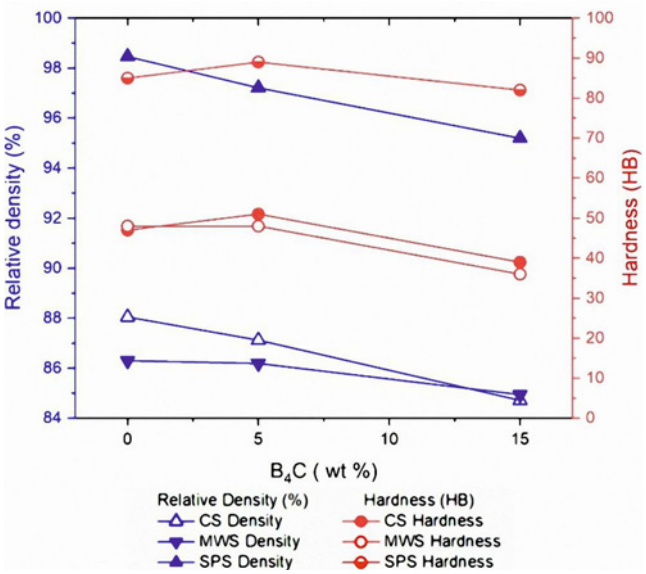


Fig. 4. Density and hardness changes in samples sintered with different techniques.

the addition of $B_4C$ particles, an increase in porosity was determined, as seen in Fig. 3, and a decrease in density, as seen in Fig. 4. This decrease in densities is attributed to the pores between the matrix powder grains and $B_4C$ and/or $B_4C$ particles [7, 18, 40]. 5 wt.% $B_4C$ added to the samples did not cause a significant decrease in density. In the samples to which 5 wt.% $B_4C$ was added, the highest density decrease was determined in the SPS sample, with a decrease of approximately 1.26 %. The pores in the microstructure of pure Alumix® 231 samples produced with the CS and MWS technique provide the spaces where $B_4C$ particles will be positioned. However, the porosity rate in the pure Alumix® 231 sample produced with the SPS technique is approximately 1.5 %, and the addition of 5 wt.% $B_4C$ caused more porosity in this sample than in the CS and MWS-coded samples. If the micrographs in Fig. 3 are examined: In samples with $B_4C$ particle addition, it is seen that the size and volume ratio of the pores formed between the particle/matrix increases with the increasing $B_4C$ particle ratio. When the density values of samples produced with different sintering techniques are compared, it can be seen in Fig. 4 that the samples produced with SPS give the highest density values. Densities over 95 % were obtained in samples produced with SPS. Compared to CS and MWS, low temperature (450 °C) and sintering time (5 min) were applied in the SPS technique. Despite applying low temperature (450 °C) and time (5 min) in sintering, compacts with low porosity and high density were obtained with the SPS technique. In the SPS technique, 50 MPa pressure is applied during sintering, and local melting occurs due to sparks. The applied pressure and local melting cause particle arrangement, neck formation between particles, acceleration and/or increase of atomic diffusion, formation of a good interface between grains, and a denser microstructure. Samples produced with CS and MWS techniques gave similar density values.

When the hardness data in Fig. 4 is examined, CS and MWS samples give hardness values that are close to each other and have similar tendencies, in line with the density data. In these samples, adding 5 wt.% $B_4C$ did not cause a significant change in hardness. Although the added hard $B_4C$ ceramic particles were expected to increase the hardness, the presence of these particles in the pores in the microstructure caused a low increase of 7.5 % in the hardness of the sample coded 5-CS-555/60. No change was observed in the hardness of the sample coded 5-MWS-555/15. Due to the increase in pore sizes and volume ratio caused by adding 15 wt.% $B_4C$, the hardness of the samples coded 15-CS-555/60 and 15-MWS-555/15 decreased by 17 and 25 %, respectively. The fact that samples produced with CS and MWS techniques give hardness and density values close to each other is an important advantage offered by MWS samples produced by holding 15 min at the high heating rate and sintering temperature in terms of time and energy saving. Samples produced with the SPS technique gave ≈ 80 % higher hardness values than samples produced with CS and MWS. wt.% $B_4C$ caused a ≈ 5 % increase in hardness, and the addition of 15 wt.% $B_4C$ caused a ≈ 3.5 % decrease in hardness compared to the sample coded SPS-450/5. The decrease in hardness in the sample coded 15-SPS-450/5 is related to the correlation between the pore volume ratio and size and the hardness of $B_4C$ particles. Ozer et al. [18, 40] stated that the increase in pore size and/or pore amount with the addition of $B_4C$ caused this decrease in hardness.

### *3.3. Electrical conductivity*

I-V measurements of the samples were made at room temperature (300 K). The electrical conductivity values of the samples are given as % IACS (International Annealed Copper Standard) in Fig. 5. The electrical resistance ($\rho$) and electrical conductivity ($\sigma$) of the samples were calculated using Eqs. (1) and (2). Electrical conductivity data calculated as $Sm^{-1}$ was converted to % IACS. Samples produced with SPS exhibited higher electrical conductivity than samples produced with CS and MWS (Fig. 5). The reason for the higher electrical conductivity in samples produced with SPS is the high density and low porosity. Samples produced with CS and MWS gave similar electrical conductivity values due to the close porosity ratio. Porosity in samples produced with MWS is approximately 2 % higher than in CS-coded samples, and electrical conductivity is approximately 4 % poorer. Electrical conductivities decreased as the weight per-

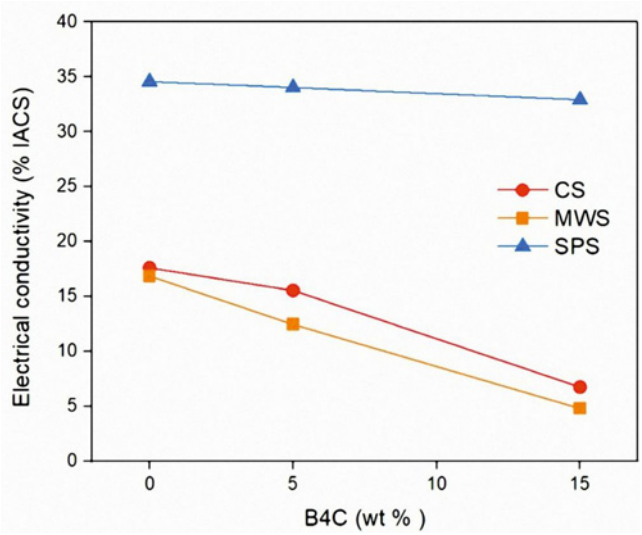


Fig. 5. Electrical conductivity plot of the samples at room temperature.

centage of $B_4C$ increased in all samples. The fact that $B_4C$ is a semiconductor and the porosity it causes in the microstructure can be the reason for this decrease in electrical conductivity [19].

The decrease in electrical conductivity is lower in SPS-coded samples. Since the porosity rate caused by $B_4C$ in the microstructure is less, the decrease in electrical conductivity in these samples was limited to ≈4.7 %. The decrease in electrical conductivity with the addition of $B_4C$ is approximately 11.7 %, 61.7 %, 26 %, and 71 %, respectively, in samples coded 5-CS-555/60, 15-CS-555/60, 5-MWS-555/15, and 15-MWS-555/15.

In general, the electrical conductivity of pure metals tends to decrease when mixed with other elements [41]. With increasing $B_4C$ weight percentage, the proportion of voids formed at the particle/matrix interface and between semiconductor $B_4C$ particles also increases. These holes serve as electron scattering sources and reduce the speed and free path length of electrons [19, 42, 43]. In addition, the energy of electrons colliding with $B_4C$ particles decreases due to their scattering. The increase in $B_4C$ particles per unit volume makes these effects evident [19]. It can be said that this is another reason for the decrease in electrical conductivity in composites containing 15 wt.% $B_4C$. All these negative effects caused by the increase in the weight percentage of $B_4C$ in the matrix caused the electrical conductivity of the samples to decrease. Electrons move by colliding with crystal defects and secondary phases (particles) in the microstructure. These collisions negatively affect the mobility of electrons. As a result, electron drift speed and electrical conductivity decrease.

## 4. Conclusions

The results of this experimental study are summarized below:

– The microstructures of all samples consist of elemental Al grains, master alloy grains, and primary Si particles. CS and MWS samples gave porosity values close to each other. The superiority of the MWS technique over the CS technique is its high heating rate, short holding time, and energy saving.

– Samples produced with CS and MWS techniques gave similar density values. The samples with the highest density are those produced with SPS.

– The addition of 5 wt.% $B_4C$ did not cause a significant change in hardness. The addition of 15 wt.% $B_4C$ caused a decrease in the hardness of samples produced with CS and MWS. Samples produced with the SPS technique gave approximately 80 % higher hardness values.

– Samples produced with SPS gave higher electrical conductivity values than samples produced with CS and MWS. Electrical conductivities decreased as the weight percentage of $B_4C$ increased in all samples.

– P/M samples produced with the SPS technique exhibited better microstructures than MWS and CS samples and provided very good data regarding density, hardness, and electrical conductivity. For this reason, P/M compact samples with good electrical conductivity and mechanical properties can be produced using the SPS technique. The fact that sintering temperature and holding time parameters are much lower in the SPS technique compared to MWS and CS techniques offers significant advantages in terms of energy and time-saving.

## References

[1] V. Khanna, V. Kumar, S. A. Bansal, Mechanical properties of aluminium-graphene/carbon nanotubes (CNTs) metal matrix composites: Advancement, opportunities and perspective, Mater. Res. Bull. 138 (2021) 111224. https://doi.org/10.1016/j.materresbull.2021.111224

[2] V. Puchy, M. Podobova, R. Dzunda, P. Hvizdos, O. Velgosova, M. Besterci, B. Ballokova, Graphene nanoplatelets reinforced aluminum alloy matrix composites produced by spark plasma sintering, Kovove Mater. 59 (2021) 237–244. https://doi.org/10.4149/km_2021_4_237

[3] W. G. E. Mosher, G. J. Kipouros, W. F. Caley, I. W. Donaldson, D. P. Bishop, On hot deformation of aluminium–silicon powder metallurgy alloys, Powder Met. 54 (2011) 366–375. https://doi.org/10.1179/003258910X12678035166773

[4] D. Kumar, R. K. Phanden, L. Thakur, A review on environment friendly and lightweight magnesium-based metal matrix composites and alloys, Mater. Today-Proc. 38 (2021) 359–364. https://doi.org/10.1016/j.matpr.2020.07.424

[5] A. Kareem, J. A. Qudeiri, A. Abdudeen, T. Ahammed, A. Ziout, A review on AA 6061 metal matrix composites produced by stir casting, Materials 14 (2021) 175. https://doi.org/10.3390/ma14010175
[6] N. Ahamad, A. Mohammad, M. L. Rinawa, K. K. Sadasivuni, P. Gupta, Correlation of structural and mechanical properties for Al-$Al_2O_3$-SiC hybrid metal matrix composites, J. Compos. Mater. 55 (2021) 3267–3280. https://doi.org/10.1177/00219983211011537
[7] M. Ozer, S. I. Aydogan, H. Cinici, A. Ozer, Effects of sintering techniques and parameters on microstructure and mechanical properties of Al-15Si-2.5Cu-0.5Mg compacts and Al-15Si-2.5Cu-0.5Mg/$B_4C$ composites, Materials Today Communications 30 (2022) 103192. https://doi.org/10.1016/j.mtcomm.2022.103192
[8] N. Kang, M. El-Mansori, A new insight on induced-tribological behaviour of hypereutectic Al-Si alloys manufactured by selective laser melting, Tribology International 149 (2020) 105751. https://doi.org/10.1016/j.triboint.2019.04.035
[9] E. Damavandi, S. Nourouzi, S. M. Rabiee, R. Jamaati, A. A. Tiamiyu, J. A. Szpunar, Effects of prior ECAP process on the dynamic impact behaviors of hypereutectic Al-Si alloy, Mat. Sci. Eng. A-Struct. 793 (2020) 139902. https://doi.org/10.1016/j.msea.2020.139902
[10] M. Faraji, A new approach in numerical modeling of inoculation of primary silicon in a hypereutectic Al-Si alloy, Metall. Mater. Trans. B 52 (2021) 778–791. https://doi.org/10.1007/s11663-020-02052-y
[11] T. T. Saravanana, M. Kamaraj, S. C. Sharma, S. Anoop, S. K. Manwatkar, K. V. Ravikanth, A. Venugopal, S. Kumaran, Influence of characteristic eutectic free microstructure on mechanical and corrosion response of spark plasma sintered hypereutectic Al-Si alloy, Mater. Lett. 308 (2022) 131104. https://doi.org/10.1016/j.matlet.2021.131104
[12] S. C. Tjong, Z. Y. Ma, Microstructural and mechanical characteristics of in situ metal matrix composites, Materials Science and Engineering: Reports 29 (2000) 49–113. https://doi.org/10.1016/S0927-796X(00)00024-3
[13] J. W. Kaczmar, K. Pietrzak, W. J. Wlosinski, The production and application of metal matrix composite materials, Mater. Process. Tech. 106 (2000) 58–67. https://doi.org/10.1016/S0924-0136(00)00639-7
[14] R. M. German, Powder Metallurgy and Particulate Materials Processing, Metal Powder Industry, Princeton, New Jersey, 2005, pp. 233–274. ISBN: 0976205718
[15] R. M. German, Sintering: From Empirical Observations to Scientific Principles, Butterwortf-Heinemann, Massachusetts, 2014, pp. 387–408. ISBN: 978-0-12-401682-8
[16] S-J. L. Kang, Sintering Densification, Grain Growth, and Microstructure, Butterworth-Heinemann, Oxford, 2005, pp. 197–205. ISBN: 978-0-7506-6385-4
[17] Y. Kaplan, S. Aksöz, H. Ada, E. İnce, S. Özsoy, The effect of aging processes on tribo-metallurgy properties of Al based ternary alloys product by P/M technique, Sci. Sinter. 52 (2020) 445–456. https://doi.org/10.2298/SOS2004445K
[18] M. Ozer, S. I. Aydogan, A. Ozer, H. Cinici, E. Ayas, Influence of spark plasma sintering and conventional sintering on microstructure and mechanical properties of hypereutectic Al-Si alloy and hypereutectic Al-Si/$B_4C$ composites, Kovove Mater. 60 (2022) 171–179. https://doi.org/10.31577/km.2022.3.171
[19] A. Ozer, H. Cetin, Correlation of microstructure, hardness, and electrical conductivity of hypereutectic Al-Si/$B_4C$ composites manufactured by hot pressing technique and subjected to hot extrusion, Can. Metall. Quart. 63 (2024) 350–359. https://doi.org/10.1080/00084433.2023.2212577
[20] Z. Pakiela, K. Ludwichowska, J. Ferenc, M. Kulczyk, Mechanical properties and electrical conductivity of Al 6101 and 6201 alloys processed by hydro-extrusion, IOP Conf. Ser.-Mat. Sci. Eng. 63 (2014) 012120. https://doi.org/10.1088/1757-899X/63/1/012120
[21] P. B. Allen, W. H. Butler, Electrical conduction in metals, Phys. Today 31 (1978) 44–49. https://doi.org/10.1063/1.2994869
[22] J. Zeng, C. Zhu, W. Wang, X. Li, H. Li, Evolution of primary Si phase, surface roughness and mechanical properties of hypereutectic Al-Si alloys with different Si contents and cooling rates, Phil. Mag. Lett. 100 (2020) 581–587. https://doi.org/10.1080/09500839.2020.1824081
[23] W. Chen, Y. Liu, H. Peng, J. Wang, W. Su, Effect of strontium and melt purification on the solidification microstructure of hypereutectic Al-Si alloys, Mater. Today Communications 34 (2023) 105310. https://doi.org/10.1016/j.mtcomm.2022.105310
[24] C. Ding, H. Hao, Z. Lu, C. Yu, X. Wu, P. Yu, S. Ye, Fabrication of hypereutectic Al-Si alloy with improved mechanical and thermal properties by hot extrusion, Mater. Charact. 202 (2023) 113026. https://doi.org/10.1016/j.matchar.2023.113026
[25] B. V. Ramnath, C. Elanchezhian, M. Jaivignesh, S. Rajesh, C. Parswajinan, A. S. A. Ghias, Evaluation of mechanical properties of aluminium alloy-alumina-boron carbide metal matrix composites, Mater. Des. 58 (2014) 332–338. https://doi.org/10.1016/j.matdes.2014.01.068
[26] A. Tuncer, B. Tasdelen, G. Arslan, Effect of passivation and precipitation hardening on processing and mechanical properties of $B_4C$-Al composites, Ceram. Int. 37 (2011) 2861–2867. https://doi.org/10.1016/j.ceramint.2011.05.007
[27] D. W. Heard, I. W. Donaldson, D. P. Bishop, Metallurgical assessment of a hyper eutectic aluminum-silicon P/M alloy, J. Mater. Process. Tech. 209 (2009) 5902–5911. https://doi.org/10.1016/j.jmatprotec.2009.07.007
[28] H. Rudianto, S. Yang, K.-W. Nam, Y.-J. Kim, Mechanical properties of Al-14Si-2.5Cu-0.5Mg aluminum-silicon P/M alloy, Review of Advanced Materials Science 28 (2011) 145–149
[29] S. S. Su, I. T. H. Chang, W. C. H. Kuo, Effects of processing conditions on the sintering response of hypereutectic Al-Si-Cu-Mg P/M alloy, Mater. Chem. Phys. 139 (2013) 775–782. https://doi.org/10.1016/j.matchemphys.2013.02.031
[30] A. Ozer, The microstructures and mechanical properties of Al-15Si-2.5Cu-0.5Mg/(wt.%)$B_4C$ composites produced through hot pressing technique and subjected to hot extrusion, Mater. Chem. Phys. 183 (2016) 288–296.

https://doi.org/10.1016/j.matchemphys.2016.08.029
[31] I. Arribas, J. M. Martin, F. Castro, The initial stage of liquid phase sintering for an Al-14Si-2.5Cu-0.5Mg (wt.%) P/M alloy, Mat. Sci. Eng. A 527 (2010) 3949–3966. https://doi.org/10.1016/j.msea.2010.02.078
[32] S. Rudinsky, J. M. Aguirre, G. Sweet, J. Milligan, D. P. Bishop, M. Brochu, Spark plasma sintering of an Al-based powder blend, Mat. Sci. Eng. A 621 (2015) 18–27. https://doi.org/10.1016/j.msea.2014.10.056
[33] A. Manonukul, A. Salee, Relationship between atmospheric dew point and sinterability of Al-Si based alloy, J. Mater. Sci. Technol. 29 (2013) 70–76. https://doi.org/10.1016/j.jmst.2012.11.010
[34] M. Oghbaei, O. Mirzaee, Microwave versus conventional sintering: A review of fundamentals, advantages and applications, J. Alloy Compd. 494 (2010) 175–189. https://doi.org/10.1016/j.jallcom.2010.01.068
[35] R. Roy, D. Agrawal, J. Cheng, S. Gedevanishvili, Full sintering of powdered-metal bodies in a microwave field, Nature 399 (1999) 668–670. https://doi.org/10.1038/21390
[36] D. Demirskyi, D. K. Agrawal, A. Ragulya, Neck formation between copper spherical particles under single-mode and multimode microwave sintering, Mat. Sci. Eng. A 527 (2010) 2142–2145. https://doi.org/10.1016/j.msea.2009.12.032
[37] J. Sun, W. Wang, Q. Yue, Review on microwave-matter interaction fundamentals and efficient microwave-associated heating strategies, Materials 9 (2016) 231. https://doi.org/10.3390/ma9040231
[38] N. Saheb, Z. Iqbal, A. Khalil, A.S. Hakeem, N-A. Aqeeli, T. Laoui, A. Al-Qutub, R. Kirchner, Spark plasma sintering of metals and metal matrix nanocomposites: A review, Journal of Nanomaterials 2012 (2012) 983470. https://doi.org/10.1155/2012/983470
[39] Z. Shen, M. Johnsson, Z. Zhao, M. Nygren, Spark plasma sintering of alumina, J. Am. Ceram. Soc. 85 (2002) 1921–1927. https://doi.org/10.1111/j.1151-2916.2002.tb00381.x
[40] M. Ozer, Y. Kaplan, A. Ozer, S. Aksoz, Influence of different sintering techniques on the wear properties of Al-15Si-2.5Cu-0.5Mg/$B_4C$ composites, Sci. Sinter. 56 (2024) 269–283. https://doi.org/10.2298/SOS231003060O
[41] H. Pal, V. Sharma, Mechanical, electrical, and thermal expansion properties of carbon nanotube-based silver and silver-palladium alloy composites, Int. J. Min. Met. Mater. 21 (2014) 1132–1140. https://doi.org/10.1007/s12613-014-1019-1
[42] O. Altuntas, M. Ozer, G. Altuntas, A. Ozer, Investigation of the microstructure, hardness and electrical conductivity properties of Fe/Graphene compacts, Mater. Sci. Tech. 39 (2023) 2670–2679. https://doi.org/10.1080/02670836.2023.2213554
[43] M. J. Isfahani, F. Payami, M. A. Asadabad, A. A. Shokri, Investigation of the effect of boron carbide nanoparticles on the structural, electrical, and mechanical properties of Al-$B_4C$ nanocomposites, J. Alloy Compd. 797 (2019) 1348-1358. https://doi.org/10.1016/j.jallcom.2019.05.188